Extending optics to 50 nm and beyond with immersion lithography

M. Switkes,[a] R. R. Kunz, M. Rothschild, and R. F. Sinta
Lincoln Laboratory, Massachusetts Institute of Technology, Lexington, Massachusetts 02420

M. Yeung and S.-Y. Baek
Department of Manufacturing Engineering, Boston University, Brookline, Massachusetts 02446

(Received 7 July 2003; accepted 15 September 2003; published 5 December 2003)

Numerical imaging simulations demonstrate the capability of immersion lithography to print features smaller than 45 nm (35 nm) with good depth of focus at a vacuum wavelength of 193 nm (157 nm). The optical impact of index variation of the immersion liquid is simulated and found to be a shift of focus of 1 nm for each 1 ppm change in the bulk index of the liquid. For an index which varies through the thickness of the liquid (e.g., due to nonuniform temperature), the focus shift is found to be proportional to the total change in optical path length (OPL), with a 1 nm change in OPL leading to a ~1.5 nm focus shift at 1.3 numerical aperture. A focus offset of 1–3 nm can be expected due to heating during scanning exposure. The possible formation of nanobubbles at resist surfaces is also discussed. While simulations show that even 10 nm thick bubbles at the surface of the resist cause 30% modulation in the aerial image intensity, no evidence of bubbles is seen in open frame immersion exposures. Imaging of 100 nm features is shown using an immersion contact phase-edge technique, with no evidence of bubbles or adverse liquid–resist interactions. Finally, we describe progress in the search for low absorbance liquids for use at 157 nm. Liquid purity, including dissolved O_2 and H_2O, is found to be critical. The current absorbance record, $0.64\pm0.07\ \mathrm{cm}^{-1}$, held by perfluorotriglyme ($CF_3[OCF_2CF_2]_3OCF_3$), is enough for a 350 μm working distance at 95% transmission. [DOI: 10.1116/1.1624257]

I. INTRODUCTION

Immersion microscopy was invented over 150 years ago when the benefit of filling the space between the microscope's final optical element and its target with a high index liquid was realized. Because the wavelength of light in a fluid is reduced from the vacuum wavelength λ, the resolution W can be improved by a factor of the index of refraction of the fluid n:

$$W=k_1\frac{\lambda/n}{\sin\theta}, \tag{1}$$

where θ is the angular half aperture of the lens and k_1 is the resolution coefficient. The idea of applying the benefits of immersion to projection lithography is likewise not new. Immersion lithography had emerged in the patent literature[1] by 1984 and in regular open literature[2] by 1987. Several small scale studies of immersion patterning[3–6] were undertaken in the 1980s and early 1990s but did not progress beyond the proof-of-concept stage; other factors on the right-hand side of Eq. (1) presented easier targets for resolution improvement. Now, with both $\sin\theta$ and k_1 approaching 85% of their physical limits, and a lack of transparent optical materials below ~150 nm that provides serious technical challenges to further reduction of λ, immersion has become a serious candidate for extending optical lithography to 50 nm and below.

Beyond improvements in resolution, immersion is attractive because the vacuum wavelength of the radiation remains unchanged, allowing much of the technology developed for dry lithography at that wavelength to be carried over into immersion. Light sources, optical materials and coatings, purging and contamination control systems, and perhaps even resists can be used essentially unchanged. Masks will likewise remain unchanged except for the reduction in feature size allowed by the improved system resolution. The novel elements in immersion lithography are essentially three. First, a new lens design is required to take advantage of the immersion liquid. Several designs for full-field immersion lenses with numerical aperture (NA)$=n\sin\theta$ up to 1.2 have been presented[7,8] by lithographic tool makers. Second, a liquid dispensing and recovery system is required, and several concepts for this have also been proposed[7,9] and are currently under study.

The final and perhaps most critical element of immersion lithography is the immersion liquid itself. As a component of a high-precision optical system as well as of the entire semiconductor process flow, the liquid must fulfill many requirements. Physically, it must be transparent at the exposure wavelength, have a high enough index to make the resolution improvement worthwhile, and have low viscosity to facilitate high speed scanning. Additionally, the liquid should be nontoxic and must be compatible with cleanroom processing. For all of these reasons, water is a very attractive candidate liquid at 193 nm. It has low absorbance,[10] $\alpha=0.036\ \mathrm{cm}^{-1}$ (base 10) and a relatively high index,[11] $n=1.44$, along with low viscosity and familiarity in the semiconductor manufacturing process. In addition to its physical properties, the immersion liquid must be chemically compatible with the photoresist and with the final lens element. It must not interact with the photoresist in any way which impedes high resolu-

[a]Electronic mail: mswitkes@ll.mit.edu

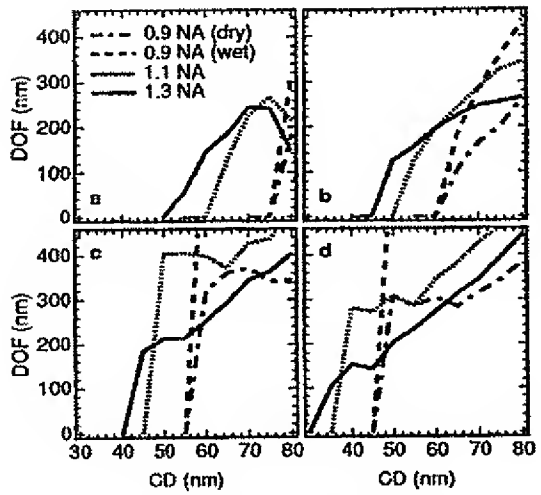

FIG. 1. Numerical simulations of printing dense line and space patterns for NAs of 0.9 (immersion and dry), 1.1, and 1.3. The depth of focus at 10% exposure latitude is shown as a function of the feature size. (a) Binary mask at 193 nm with annular illumination (σ=0.4–0.6). (b) Binary mask at 157 nm with annular illumination. (c) Alternating phase shift mask at 193 nm with conventional illumination (σ=0.3). (d) Alternating phase shift mask at 157 nm.

tion imaging, and must not contaminate the lens over the life of the exposure tool.

In this article, we address further concerns about the homogeneity of the liquid index due to temperature variations as well as the possibility of bubble formation in the liquid. We also report our initial imaging results using water immersion phase-edge contact printing. At 157 nm, research has focused on identifying suitably transparent fluids. Fluorinated fluids have shown some promise as immersion liquids,[12] but absorbance has remained too high to permit practical working distances. Here we report on our progress in identifying and purifying suitable fluorinated liquids for use at 157 nm.

II. IMAGING SIMULATIONS

To assess the potential of immersion lithography, we performed numerical imaging simulations using the model described fully in Ref. 13 to calculate exposure-defocus trees for dense line and space patterns with a ±10% critical dimension (CD) tolerance. This Maxwell vector model accounts for thin-film interference as well as polarization and other high NA effects, and all simulations assume randomly polarized light. Figure 1 shows the depth of focus (DOF) as a function of the nominal linewidth for an exposure latitude of 10%, for conventional dry lithography with NA=$n \sin\theta$ of 0.9 and water immersion lithography with NAs of 0.9–1.3, both using annular illumination at σ=0.4–0.6. At λ=193, 0.9 NA has essentially no DOF below 75 nm with a simple binary mask while water immersion with the same value of $\sin\theta$ (NA=1.3) allows printing with good DOF below 60 nm [Fig. 1(a)]. At λ=157, the improvement is similar with NA=1.3 allowing printing below 50 nm compared to the 65 nm available with ultrahigh NA dry lithography [Fig. 1(b)]. Resolution can be further improved using the whole suite of resolution enhancement techniques developed for dry lithography which carry over directly into immersion. For example, using an alternating phase shift mask (altPSM) with conventional illumination (σ=0.3), immersion allows λ=193 to extend to 45 nm features and λ=157 to 35 nm features as seen in Figs. 1(c) and 1(d). We note that, according to the *International Technology Roadmap for Semiconductors* (Semiconductor Industry Association, San Jose, CA, 2002, http://public.itrs.net/), 45 nm lithography will be needed starting in the year 2010, and 32 nm lithography starting in 2013. Even in the absence of the highest NAs, immersion will allow printing down to ~50 nm at 193 nm using NAs for which full-field lens designs are currently available.[7,8]

III. INDEX VARIATION DUE TO HEATING

One major concern in immersion lithography is distortion of the image due to index inhomogeneities in the liquid. Variation in the index of the immersion fluid causes, to first order, defocus in the image,[14] along with small amounts of spherical and higher order abberations.[13] With a 1 mm working distance and $\sin\theta$=0.9, our simulations show that a change in the bulk liquid index of 1 ppm causes ~1 nm of defocus. Because the thermo-optic coefficient of water[11] at 193 nm, $dn/dT=-10^{-4}/°C$, is about 20 times higher than that of the traditional N_2 ambient, liquid temperature control is critical. Each 0.01 °C uncertainty in the bulk water temperature reduces the focus budget by ~1 nm.

During exposure, the wafer absorbs photons and heats up, and some of this heat is transferred to the immersion liquid. Numerical modeling of this heating process must take into account the scanning of the wafer which results in a liquid flow, which replaces heated liquid with fresh liquid under the lens. Some results of such a detailed numerical model[9] are reproduced in Fig. 2(a), which shows temperature profiles of the liquid at the trailing edge of the exposure slit for various flow conditions. While the temperature rises as much as 0.15 °C near the wafer surface in water immersion, the heat does not have time to diffuse throughout the bulk of the liquid. Its impact is thus much smaller than a similar shift in the bulk temperature. The temperature induced change in the optical path difference (OPD) between the axial and marginal rays is

$$\Delta\mathrm{OPD}=\Delta\mathrm{OPL}_{\mathrm{axial}}-\Delta\mathrm{OPL}_{\mathrm{marginal}}=\frac{dn}{dt}\left(\frac{1}{\cos\theta}-1\right)\int_{\mathrm{wafer}}^{\mathrm{lens}}\Delta T\,dz, \tag{2}$$

where ΔOPL is the change in optical path length (OPL) of each ray. The same ΔOPD can also be induced by moving the wafer plane out of focus:

$$\Delta\mathrm{OPD}=n(\cos\theta-1)\Delta\mathrm{focus}. \tag{3}$$

Combining Eqs. (2) and (3), we see that the equivalent focus shift for a coherent imaging system is

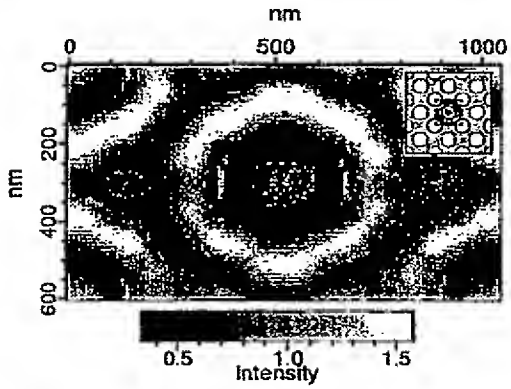

FIG. 3. Simulated aerial image of an array of gas bubbles 300 nm in diameter and 100 nm high on the resist surface. The spatial modulation of the intensity is 80%. Inset: Schematic of the gas bubble array. The shaded area in the center represents the area shown in the main part.

incident dose, with no thresholding behavior. Within the dose accuracy, the thickness removed was equal for wet and dry exposures. Atomic force microscope (AFM) inspection of the developed surfaces [Figs. 4(a) and 4(b)] showed little difference between wet and dry and certainly no evidence of bubbles at any dose. The Fourier spectral signature of the surface roughness [Fig. 4(c)] also revealed no significant difference between the dry and immersion exposures across the dose range measured.

V. CONTACT IMAGING

Another area of concern in immersion lithography is the possibility of interaction of the immersion liquid with the resist. Preliminary tests with blanket exposures suggest that, at least for some types of 193 nm resist, exposure to water

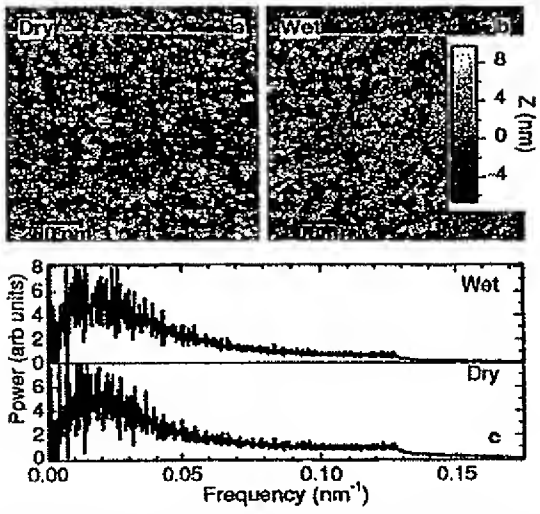

FIG. 4. AFM images of a gray tone resist exposed at 193 nm under (a) N_2 and (b) water ambient. No evidence of bubbles is seen. (c) The power spectral density of the surface roughness is virtually identical after wet and dry exposure.

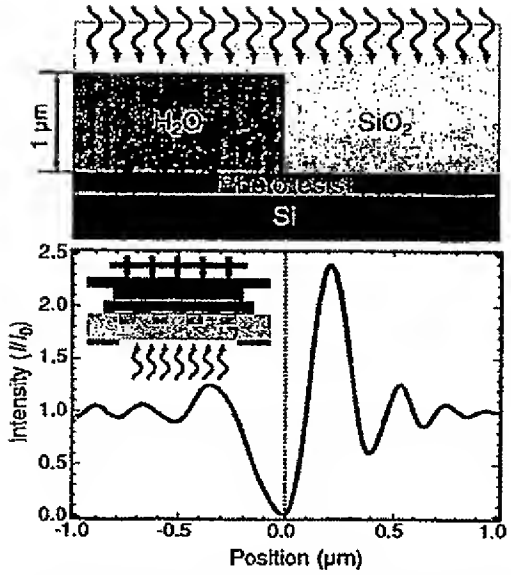

FIG. 5. Top: Schematic of the immersion phase-edge contact printing process. The relief in the phase mask is filled with water. Bottom: Simulated aerial image at the phase edge. Inset: Schematic of the simple jig used to achieve optical contact between the wafer and the mask. An array of fine pitched screws apply pressure, while the fringes are observed through the mask from below.

causes little to no change in resist thickness or surface energy.[14] Recently, we have performed a series of experiments which determined the elemental composition of 193 nm photoresists exposed to water with and without irradiation. These x-ray photoelectron spectroscopy (XPS) studies showed, among other effects, that water soluble base stabilizers are leached out of the resist almost immediately upon contact with water. However, the impact of such changes in resist composition on lithographic performance is still unclear. There is no substitute for high resolution imaging. In the absence of an immersion projection tool, we have adapted a phase-edge contact printing technique[19] which enables the patterning of sub-100 nm features with a simple apparatus. A jig consisting of an array of fine pitched screws (Fig. 5 inset) is used to bring a water covered, resist-coated wafer into optical contact with a fused silica phase mask. Using interference fringes as a guide, good contact can be established over almost all of the 50×50 mm^2 exposure area. Because this procedure is not carried out in a clean environment, a few dust particles typically create localized (1–3 mm diam) areas of poor contact. The resist is then exposed through the mask. Because water fills the relief of the mask, phase edges must be etched to a depth d which yields an optical path difference, $\mathrm{OPD}=d(n_{\mathrm{mask}}-n_{\mathrm{liquid}})=\lambda/2$ between the light transmitted through the glass and that transmitted through the water; with a fused silica mask at 193 nm, $d\approx 1\ \mu$m. A diagram of the contact at a single phase edge as well as a numerical simulation of the resulting aerial image are shown in Fig. 5. This technique easily yields features with ~100 nm linewidths. Figure 6 shows scanning electron microscope (SEM) micrographs of exposures of a 300 nm

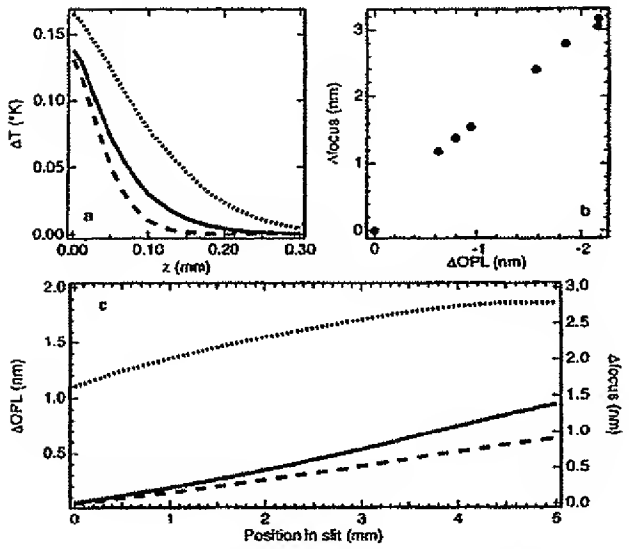

FIG. 2. Numerical modeling of the effect of temperature gradients in the fluid. (a) Temperature gradients at the trailing edge of a water immersion exposure slit (after Ref. 9). The dashed line represents fluid injection at 1 kPa parallel to the scan direction, the dotted line at 1 kPa antiparallel to the scan, and the solid line at 0 Pa. The wafer is at $z=0$ and the lens surface at $z=1$ mm. (b) Numerically modeled focus shift due to temperature gradients as a function of the integrated change in optical path length. (c) Optical path length and focus differences across the 5 mm exposure slit. The leading edge is at 0 and the trailing edge, corresponding to the gradients shown in (a), is at 5 mm.

$$\Delta\text{focus} = -\frac{\Delta\text{OPL}_{\text{axial}}}{n\cos\theta} = -\frac{\Delta\text{OPL}_{\text{axial}}}{\sqrt{n^2-\text{NA}^2}}. \tag{4}$$

For water immersion at NA=1.3, $\Delta\text{focus} = -1.6\,\Delta\text{OPL}_{\text{axial}}$. These analytical results were confirmed by numerical simulations in which the liquid was broken into layers and the index of each layer adjusted to match these one-dimensional (1D) temperature profiles. The resulting shift in best focus, shown in Fig. 2(b), is $-1.5\,\Delta\text{OPL}_{\text{axial}}$ with the difference from the analytical results due to the partial coherence modeled in the simulations. In reality, a temperature profile also induces spherical aberrations of various orders but they are quite small. Even the most extreme temperature gradients simulated showed no change in contrast at best focus. For realistic scanning parameters, total focus shifts of 1–3 nm can be expected, depending on the flow conditions. This shift constitutes a small but nonnegligible portion of the focus budget.

The temperature profile in the liquid is, of course, not one dimensional, even in the case of uniform illumination. The primary two-dimensional (2D) effect is the difference in temperature between the leading and trailing edges of the exposure slit. The fluid at the trailing edge has absorbed more energy and has had more time for the heat to propagate. It is thus hotter through more of its thickness than the liquid at the leading edge which remains near the ambient temperature. This results in a difference in focus (tilt) across the 5 mm slit of approximately the same magnitude as the overall focus offset [Fig. 2(c)]. We have recently extended our optical simulation capability to take this 2D temperature profile into account, and our initial results are in agreement with the estimates based on 1D results shown here.

A final possible source of heating which has not yet been considered is the viscous heating caused by flow. This should be a small effect for water, but may be significant for other liquids such as those under study for use at 157 nm, and may indeed prove to be the most important factor limiting acceptable liquid viscosity.

IV. BUBBLES

The exposure ambient of a conventional lithographic exposure system is a gas where spatial inhomogeneities due to changes in pressure or composition are small. In immersion lithography, however, there is the possibility of large index inhomogeneity due to bubbles in the immersion liquid. Microscopic bubbles (~10 μm and larger) can be formed in the liquid handling system by entraining gas from the outside during scanning[15] or by devolution of dissolved gas due to temperature or pressure changes in the liquid. The former can be avoided by careful fluidic design and the latter by removing the dissolved gas from the water (degassing). Bubbles could also arise from the outgassing of resists under exposure. Using conservative estimates: free diffusion of gas from the resist into the water, a high peak outgassing rate (10^{15} molecules $\text{cm}^{-2}\,\text{s}^{-1}$; equivalent to the IBM V2 experimental resist[16]), and a high gas diffusion rate in the resist ($10^{-8}\,\text{cm}^{-2}\,\text{s}^{-1}$), the peak concentration of a common outgassing product, isobutene, in water is ~250 $\mu\text{g}\,\text{cm}^{-3}$ below but not far below the 340 $\mu\text{g}\,\text{cm}^{-3}$ solubility limit.[17] Direct experimental verification of the effect of outgassing is clearly required and experiments are ongoing at Lincoln Laboratory to measure the formation of bubbles from a variety of resists.

There is also some evidence that large numbers of nanobubbles with 10–100 nm thickness may form spontaneously at hydrophobic surfaces[18] due to the energetic advantage of having a gas layer isolating the water from the surface. The formation of such bubbles on a resist surface would be disastrous for immersion lithography. Figure 3 shows a numerical simulation of the aerial image created by blanket exposure through an array of bubbles 300 nm in diameter and 100 nm high at the surface of the resist. Instead of a uniform image, the intensity is modulated by 80%; any such bubble would almost certainly cause a printable defect. Simulations with bubbles as little as 10 nm high show 30% modulation in image intensity. It is thus critical for immersion lithography to establish whether such bubbles form at resist–liquid interfaces.

Because bubbles at the resist surface are predicted to have such a large impact on the aerial image, blanket exposures of water coated resist should reveal their presence. Wafers coated with 1 μm thick hydrophobic (unexposed water contact angle 80°) gray tone resist were exposed at doses from 1 to 1000 $\text{mJ}\,\text{cm}^{-2}$ under both N_2 and water ambient in an open frame exposure system. The thickness of resist removed upon development was proportional to the log of the

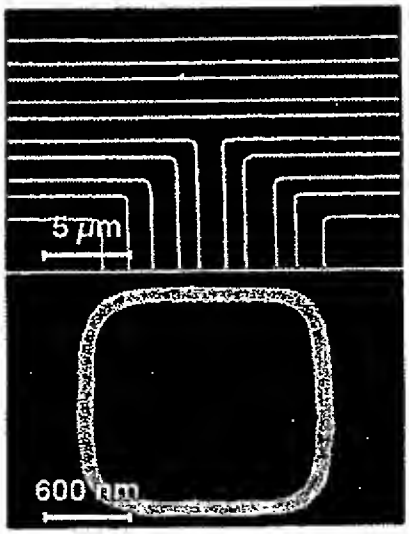

FIG. 6. SEM micrographs of 300 nm bilayer resist exposed at 193 nm with immersion phase-edge contact printing. The linewidth in both images is 100 nm.

thick bilayer resist[19] which show no evidence of defects due to bubble formation or water–resist interaction. More extensive tests of model 193 nm resists are planned along with a study of the impact of immersion liquid impurities on resist performance.

VI. FLUIDS FOR 157 nm IMMERSION

While water appears to be the preferred immersion liquid at 193 nm, fundamental work remains in the identification of a suitable fluid for 157 nm use. The primary issue and the focus of our research to date is the lack of sufficiently transparent liquids at this wavelength. Liquid absorbance is determined by measuring the transmission of cells consisting of the liquid sandwiched between two CaF_2 windows held apart by a spacer whose thickness determines the path length x in the liquid. Measurements of three cells with $x = 5\ \mu m - 1$ mm fit to Beer's law, $T = T_0 10^{-\alpha x}$, yield liquid absorbance α. The error (1σ) is on the order of 0.3 cm^{-1}, principally due to cell-to-cell differences in the transmission of the CaF_2 windows, T_0, which can vary by a few percent at 157 nm. The accuracy can be improved by an order of magnitude by measuring the same cell (i.e., the same windows) three to five times with different spacers.

Initial studies[10] focused on perfluorinated polyethers (PFPEs) which are available commercially as high performance pump oils and heat transfer fluids. The absorbance of these materials as received from their manufacturers was found to be, at best, 6 cm^{-1}, which would permit a working distance of less than 40 μm at 95% transmission. This "as received" absorbance can be reduced in several ways, for example, by the elimination of dissolved oxygen. In air, perfluorocarbon liquids dissolve large amounts of O_2 which contribute a significant portion of the overall absorbance at 157 nm. This O_2 can be removed, either by sparging with N_2 gas or by repeated cycles of freezing, pumping, and thawing under vacuum. De-oxygenated PFPEs with absorbances as low as 3 cm^{-1} were found. Even with the removal of O_2, however, nuclear magnetic resonance (NMR) and gas chromatography/mass spectrometry (GCMS) reveal these PFPEs to be complicated systems with polydisperse molecular weights and defects in the polymer backbone, making systematic study of the absorbance difficult.[14]

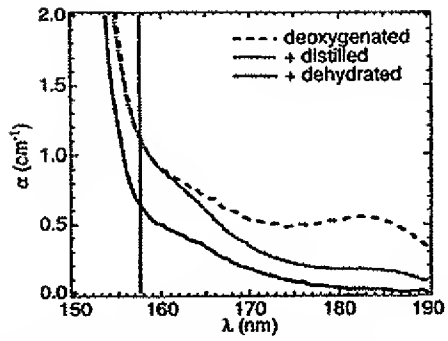

FIG. 7. Absorbance of perfluorotriglyme after de-oxygenation (dashed line), distillation followed by de-oxygenation (dotted line), and distillation followed by de-oxygenation and dehydration.

Studies of simpler perfluorocarbon and hydrofluorocarbon systems have emphasized that liquid purity is the key to low absorbance at these short wavelengths. With low molecular weight materials, routine use of GCMS can ensure that low levels of contaminants do not dominate the measured absorbances. Under these conditions, very low values of absorbance can be found. The lowest absorbance material measured to date is perfluorotriglyme (PFTG, $CF_3[OCF_2CF_2]_3OCF_3$). With the oxygen removed, PFTG has a 157 nm absorbance of 1.12 ± 0.08 cm^{-1} (Fig. 7), yielding a 200 μm working distance at 95% transmission. GCMS analysis reveals the presence of trace levels of contaminants, principally chlorofluorocarbon and unsaturated fluorocarbon species which can be partially removed by distillation. We estimate that even 1 ppm of chlorofluorocarbon can contribute ~0.5 cm^{-1} to the 157 nm absorbance. As seen in Fig. 7, while distillation improves the absorbance at longer wavelengths, the effect at 157 nm is not significant. Finally, at these low absorbances, the ppm levels of water dissolved in the perfluorocarbons are significant. When this moisture is reduced by treatment with a silica based drying agent, the 157 nm absorbance of PFTG is 0.64 ± 0.07 cm^{-1}, the current record for low absorbance of an organic liquid and low enough for a 350 μm working distance.

VII. CONCLUSIONS AND FURTHER WORK

Immersion lithography can improve the resolution of projection optics and should allow the extension of optical lithography beyond 50 nm. At 193 nm, water appears to be the immersion liquid of choice, and work is ongoing to discover potential issues with its use. To date, no show-stopping problems have been identified. Areas of concern remain, however, including bubble formation from resist outgassing, po-